TOR Complex 2 localises to the Cytokinetic Actomyosin ring and controls the fidelity of cytokinesis.

Karen Baker[3,6], Sara Kirkham[1,6], Lenka Halova[1], Jane Atkin[1], Mirita Franz-Wachtel[4], David Cobley[1], Karsten Krug[4], Boris Maček[4], Daniel P. Mulvihill[3,7] & Janni Petersen[1,2,5,7]

[1] Faculty of Life Sciences, University of Manchester, Oxford Road, Manchester, M13 9PT, United Kingdom.

[2] Flinders Centre for Innovation in Cancer, School of Medicine, Flinders University, Adelaide, SA 5001, Australia.

[3] School of Biosciences, University of Kent, Giles Lane, Canterbury, Kent, CT2 7NJ, United Kingdom.

[4] Proteome Center Tübingen, Auf der Morgenstelle 15, 72076 Tuebingen, Germany.

[5] South Australia Health and Medical Research Institute, North Terrace, PO Box 11060, Adelaide SA 5000 Australia.

[6]These authors contributed equally to this work.

[7] Authors for correspondence e-mail: d.p.mulvihill@kent.ac.uk
phone: +44 1227 827239
e-mail: Janni.Petersen@Flinders.edu.au
phone: +61 8 82044183

Key words: Rictor, TOR, TORC2 Myosin II, Myosin V, Acp1, CAPZA, Schizosaccharomyces pombe.

JCS Advance Online Article. Posted on 20 May 2016

Abstract

The timing of cell division is controlled by the coupled regulation of growth and division. The TOR signalling network synchronises these processes with the environmental setting. Here we describe a novel interaction of the fission yeast TOR Complex 2 (TORC2) with the Cytokinetic Actomyosin Ring (CAR), and a novel role for TORC2 in regulating the timing and fidelity of cytokinesis. Disruption of TORC2 or its localisation results in defects in CAR morphology and constriction. We provide evidence that a myosin II, Myp2, and myosin V, Myo51, play roles in recruiting TORC2 to the CAR. We show that Myp2 and TORC2 are co-dependent upon each other for their normal localisation to the cytokinetic machinery. We go on to show that TORC2 dependent phosphorylation of Acp1 (Actin Capping Protein, a known regulator of cytokinesis) controls CAR stability and the modulation of CAPZA/B$^{Acp1/2}$ heterodimer formation and is essential for survival upon stress. Thus TORC2 localisation to the CAR and TORC2 dependent CAPZA^{Acp1} phosphorylation contributes to timely control and fidelity of cytokinesis and cell division.

Introduction

TOR signaling plays a key role in modulating the spatial and temporal control of cell growth in response to different environmental conditions. The mTOR kinase forms two functionally distinct protein complexes TOR complex 1 (TORC1) and TORC2 (Laplante and Sabatini, 2012). TORC1 and TORC2 are defined by unique components that are highly conserved across species. TORC1 contains RAPTOR (regulatory associated protein of mTOR) and TORC2 contains Sin1 and RICTOR (rapamycin-insensitive companion of mTOR) (Wullschleger et al., 2006). It is rapamycin-sensitive TORC1 that is the major nutrient sensor, which integrates environmental cues with cell growth. TORC2 is regulated by different cues and exerts distinct functions (Laplante and Sabatini, 2012). Both TORC1 and TORC2 have been implicated in the control of cell migration and F-actin organisation (Liu and Parent, 2011). Inhibition of TORC1 with rapamycin prevents lamellipodia formation through the reduced expression of the small GTPase RhoA in mammalian cells (Liu et al., 2010). Similarly TORC2 has been shown to play a key role in regulating the organisation and polarity of the actin cytoskeleton in Saccharomyces cerevisiae, Dictyostelium discoideum and mammalian cells (Jacinto et al., 2004; Lee et al., 2005; Schmidt et al., 1996).

The fission yeast, Schizosaccharomyces pombe, contains two TOR protein kinases: Tor1 and Tor2. The majority of TORC2 contains the non-essential catalytic component Tor1 kinase (Alvarez and Moreno, 2006; Hayashi et al., 2007; Matsuo et al., 2007). Importantly, all the functional specificities of TORC1 and TORC2 are conserved in yeasts. Cells lacking TORC2 components, such as Tor1, Sin1 or the fission yeast RICTOR homolog, Ste20 (which is not a homolog of the budding yeast PAK-like kinase of the same name) are larger than wild type and are sensitive to heat, osmotic and oxidative stress. In addition these mutants are sterile as they are unable to undergo the G_1 arrest that is an essential pre-requisite for mating in fission yeast (Kawai et al., 2001; Weisman and Choder, 2001). In fission yeast, F-actin cables are thicker than wild type and the cortical actin is atypically asymmetric in tor1 deficient mutants (Ikai et al., 2011; Matsuo et al., 2007). These distinctions prompted us to explore mechanisms by which TORC2 may impact actin cytoskeletal functions in fission yeast.

Here we report a novel localisation of TORC2 to the Cytokinetic Actomyosin Ring (CAR) and a role in moderating the successful completion of cytokinesis. We describe a mechanism by which TORC2 controls CAPZA/B$^{Acp1/2}$ heterodimer formation to regulate the actin cytoskeleton, and thereby the timely control of cytokinesis and ensure survival upon changes to the extracellular environment.

Results

TORC2 controls the integrity of the Cytokinetic Actomyosin Ring.

In order to examine potential roles TORC2 may have during actin dependent cell growth and division (Lancaster and Baum, 2014) we undertook a phenotypic analysis of cells lacking Rictor, the core TORC2 specific component. The main catalytic component of TORC2 is the Tor1 protein kinase (Alvarez and Moreno, 2006; Hayashi et al., 2007; Matsuo et al., 2007), however cells lacking Tor1 are capable of incorporating Tor2 into the TORC2 complex (Matsuo et al., 2007; Hartmuth and Petersen, 2009). In contrast, deleting the fission yeast Rictor homologue, Rictor^{ste20}, from the genome specifically ablates TORC2 function within the cell. Cells lacking, Rictor^{ste20}, are elongated and display an altered cell morphology, with a cell diameter significantly greater than otherwise isogenic wild type controls (Matsuo et al., 2007; Hartmuth and Petersen, 2009) (Fig. 1A, B & S1A). Increased cell diameter and cell length is normally associated with cells in the diploid lifecycle. FACS analysis of TORC2 deficient mutants or acute Torin1 (Tor inhibitor 1) (Atkin et al., 2014) treated wild type cells revealed, the major 2N peak that is normally associated with wild type haploid fission yeast cells (Fig 1C), along with an additional minor 4N peak (Fig. 1C). Cells in the diploid lifecycle have significantly larger nuclei than haploid cells (Neumann and Nurse, 2007). The nuclei diameter were equivalent in wild type and Rictor$^{ste20}\Delta$ cells (Fig. 1D) indicating that the TORC2 deficient mutants are haploid cells with altered cell size. The minor 4N peak observed by FACS may be brought about by a small population of diploid cells. Alternatively this small peak could represent cells in the haploid life cycle delayed in cell division but which have completed the next S-phase. Division septa were often aberrant and misplaced, with the septum located away from the cell equator in 55% of Rictor$^{ste20}\Delta$ cells (these included septa positioned more than 5%, of the distance spanning the cell end to the cell equator, away from the cell equator). In contrast, none of the septa were misplaced in all observed wild type cells. Finally, elevated levels of new cell wall material was observed at the cell equator in the absence of TORC2 function (Fig. 1A, S1A). Together these data indicate TORC2 deficient haploid cells display defects in cytokinesis and cell fission.

Visualisation of septal material in Rictor$^{ste20}\Delta$ cells revealed that a large proportion of cells had misplaced or aberrant septa (Fig. 1A, S1A). myo2-mCherry cells were used to follow Cytokinetic Actomyosin Ring (CAR) localisation and dynamics. myo2-mCherry cells containing functional TORC2 displayed growth characteristics and genetic interactions equivalent to the wt myo2^{+} allele (Fig. 1E, movie 1). In contrast time-lapse imaging of

myo2-mCherry Rictor$^{ste20\Delta}$cells revealed TORC2 deficient cells remained in the phase of the cell cycle dedicated to cytokinesis for a prolonged period. As well as displaying delayed constriction, the CAR was seen to either split or collapse (39% of cells) (Fig. 1F, movie 2) or slide along the cortex (11% of cells) (Figure 1G). This is consistent with our observation that a significant proportion of septa in Rictor$^{ste20\Delta}$ cells formed septum that were more than 5% of the cell length away from the centre of the cell (Fig. S1A). In a small proportion (~ 2%) of these Rictor$^{ste20\Delta}$cells the spindle was seen to from and extend on one side of the misplaced CAR (Fig. S1B), these cells are likely to contribute to the 4N peak observed by FACS (Fig. 1C). In addition Rictor$^{ste20\Delta}$cells often failed to integrate medial Myo2 foci into stable CAR over an extended period of several hours without inhibiting cell growth (<5% of cells) (movie 3), and were also seen to complete CAR constriction, and then reform form at the division site before dividing in two (7% of cells) (movie 4). Consistent with this observation, anti-tropomyosin immunofluorescence staining of actin filaments in Rictor$^{ste20\Delta}$cells revealed defects in actin ring function during cytokinesis, with divided cells possessing an unconstructed CAR structure at the cell end at which cell division had just occurred (Fig. S1C). Thus TORC2 function is not only required to maintain normal cell size, but also plays a critical role in regulating the timing of CAR formation and maintaining its subsequent integrity during cell division.

TORC2 interacts with and localises to the Cytokinetic Actomyosin Ring during ring constriction.

In order to explore how TORC2 affects the integrity of the CAR, we undertook a proteomic-based analysis to identify proteins that co-purified with the main TORC2 catalytic component, Tor1. Mass spectrometry of Tor1 immuno-precipitates from 20 litres of early-log phase culture identified 3 known core TORC2 components (Rictor^{Ste20}, Sin1 and Pop3) as well as the TORC2 substrate Gad8 (Fig. 2A). Intriguingly, as well as co-purifying with Cdc12, a formin required for nucleation of Tropomyosin-stablised actin filaments within the CAR, in three independent experiments Tor1 co-purified with the class II and V myosin heavy chains, Myp2 & Myo51, both of which are core components of the actomyosin cytoskeleton and cytokinetic division machinery (Fig. 2A).

These links between TORC2 and control of cytokinesis prompted us to re-visit the localisation studies reporting RICTOR^{Ste20}-3GFP recruitment to the plasma membrane (Tatebe et al., 2010). Live cell imaging of myo2-mCherry RICTOR^{Ste20}-3GFP and myo51-mCherry RICTOR^{Ste20}-3GFP cells revealed TORC2 co-localised with each myosin heavy

chain at the CAR (Fig. 2B). To correlate the timing of TORC2 reorganisation and recruitment to the contractile apparatus with spindle dynamics and CAR formation, RICTOR^{Ste20}-3GFP dynamics were examined in cells expressing an mCherry labelled allele of the essential class II myosin, myo2, and tdTomato labelled version of the essential spindle pole body (SPB) component Sid4 (myo2-mCherry sid4-tdTomato cells) (Fig. 2C, Movie 5). Upon entry into mitosis, Myo2 is recruited to foci at the cell equator and the two SPBs separate juxtaposed the elongating mitotic spindle until metaphase (Fig. 2C-E – phase I, Fig. S1D). At the onset of anaphase, the spindle elongates and Myo2 foci coalesce to form the CAR (phase II) (Mulvihill and Hyams, 2002; Wu et al., 2003). It is at this time that foci of RICTOR^{Ste20}-3GFP localised to the CAR, where it remains through its subsequent constriction (phase III), and disassembly (phase IV), when it recruits to the ensuing new cell end (Fig. 2C & F, Movie 5). Thus TORC2 localises to the CAR during mitosis where it interacts with Cdc12, Myp2 and Myo51, key regulatory components of CAR formation and function.

Myosin V and myosin II regulate RICTOR^{Ste20} recruitment at the CAR.

We next decided to investigate the physical interaction between RICTOR^{Ste20} and the myosins, Myp2 and Myo51, to explore whether these actin-associated motor proteins play a role in recruiting TORC2 to the cell equator during cytokinesis. The class V myosin, Myo51, play key roles in regulating CAR function and dynamics (Bezanilla et al., 1997; Win et al., 2001). Fission yeast contains two myosin Vs, Myo51 and Myo52. The minor myosin V isoform, Myo51, localizes to the CAR (Motegi et al., 2001; Win et al., 2001) and is required for correct CAR formation (Fig. S1E). Small-scale immunoprecipitation confirmed the physical association between TORC2 and the cargo-binding domain of Myo51, as Tor1 co-purified with the Myo51 tail fused to GFP (Doyle et al, 2009) (Fig. 3A). This confirmation combined with our observation that Myo51-mCherry colocalised with RICTOR^{Ste20}-3GFP during cytokinesis (Fig. 2B) provides strong evidence that Myo51 interacts with TORC2 during cytokinesis. Consistent with this finding, RICTOR^{Ste20}-3GFP failed to localize to the ring in the absence of Myo51 (Fig. 3B,C), and localised instead to the septum as it forms around the outside edge of the constricting CAR (Fig. 3C). Removal of the second myosin V homologue through deletion of the myo52^{+} gene had no discernable impact upon RICTOR^{Ste20}-3GFP distribution (data not shown). In contrast RICTOR^{Ste20} function was not required for myosin V^{Myo51} recruitment to the CAR (Fig. 3D). Thus the recruitment of TORC2 to the CAR is dependent upon the myosin V motor, Myo51, with which it physically associates.

Like Myo51, the class II myosin Myp2, which physically interacts with Tor1 (Fig, 2A) and plays a role in maintaining the integrity of the CAR during cytokinesis. Cells lacking myp2 display cytokinesis defects (Bezanilla et al., 1997; Mulvihill et al., 2000) similar to those observed here for RICTOR$^{Ste20}\Delta$ cells. For example, the CAR sometimes split in two, and each half constrict independently of each other (Figure 3E, asterisk) (Mulvihill and Hyams, 2003). Interestingly, in the majority (> 60%) of cells lacking Myp2, RICTOR^{Ste20} did not localise to the cell equator (Fig. 3E & F). Intriguingly Myp2 was also required for RICTOR^{Ste20}-3GFP localisation to cell poles (Fig. 3E – compare lack of cell pole localisation with that observed in myp2^{+} cells, highlighted by arrow-heads in Fig. 2 & 3). Why this CAR component should affect the cortical TORC2 localisation is currently unclear, however western blot analysis confirmed persistence of RICTOR^{Ste20} protein in the *myp2*Δ cells (data not shown). To further investigate and confirm TORC2's dependence upon Myp2 for localisation and interaction with the CAR we used timelapse imaging to characterise the relative timing of spindle dynamics, CAR formation and TORC2 localisation to the cell equator. Time-lapse imaging of more than 30 prototroph wt cells revealed CAR constriction (phase III) lasted 25 min (Fig. 3F). In contrast this event took twice as long in cells lacking Myp2 (50 min), confirming the role of this protein in modulating CAR constriction (Bezanilla et al., 1997; Mulvihill et al., 2000; Huang et al., 2012). RICTOR^{Ste20}-3GFP failed to localise to the cell equator in the majority (~ 60%) of *myp2*Δ cells, and took almost twice as long as equivalent myp2^{+} cells to complete CAR constriction (phase III) (Fig. 3F, S1D). However, RICTOR^{Ste20} localised correctly in the remaining ~40% of *myp2*Δ cells, and phase III took ~50% longer to complete than wild type (Fig. 3F & S1D). Together our observations are consistent with both class II and V myosins co-purifying with TORC2 and playing a role in regulating TORC2 localisation to the CAR.

TORC2 regulate Myp2 CAR localisation and the timing of CAR constriction.

We next explored the link between TORC2 and the timing of cytokinesis further by visualising cytokinetic ring dynamics using the myosin II motor proteins, Myo2 and Myp2, in Rictor$^{ste20}\Delta$ cells. Time-lapse imaging of more than 30 Rictor$^{ste20}\Delta$ cells revealed that of those cells which formed a CAR, constriction and disassembly (Fig. 4A phase III & IV) took on average more than three times longer than in wt cells (Fig. 4A, S1A). Rictor^{ste20} only localised to the CAR in 40% of *myp2*Δ cells (Fig. 4), likewise Myp2 recruitment to the CAR was frequently aberrant in Rictor$^{ste20}\Delta$ cells (Fig. 4B,D) indicating a co-dependency. While Myp2 recruited to the CAR 10.3 min after its formation (phase II) in wild type cells and

remained there throughout CAR constriction (Fig. 4A,C, Movie 6), Myp2 CAR recruitment was extremely transient in the majority of mitotic cells lacking TORC2 RICTOR$^{Ste20}\Delta$ function (Fig. 4D). Critically, in RICTOR$^{Ste20}\Delta$ cells in which Myp2 localised to the CAR, the ring remained un-constricted for a long period (Fig. 4D & E), and the contractile apparatus was often observed sliding along the length of the cell (Figure 4D & E). Therefore TORC2 not only co-purifies with regulators of cytokinesis, ablating TORC2 function leads to defects in CAR formation and severe delays in its constriction (Fig. 4A, 1SA).

TOR dependent phosphorylation on CAPZA^{Acp1} serines 172 and 189.

To determine whether the TORC2 interacting CAR components (Fig. 2A) are substrates of the complex we examined data from a SILAC (Stable isotope labelling by amino acids in cell culture) mass spectrometric screen for phospho-peptides that showed differential phosphorylation upon Torin1 inhibition of TOR function (Atkin et al., 2014). With the exception of Ppk32 and Myo51, phosphorylation sites were identified in all co-purifying proteins. Critically, none of these sites were regulated by TOR signalling, as they remained unchanged following TOR inhibition by Torin1 (Fig S1F).

Importantly, cytokinesis and the dynamics of actin polymers are regulated, in part, by a heterodimeric complex consisting of the actin capping proteins Acp1 and Acp2 (homologues of human CAPZA and B), which binds to and stabilises the barbed end of actin structures (Yamashita et al., 2003). Interestingly, the TOR phosphorylation dependent SILAC screen revealed that CAPZA^{Acp1} displayed differentiation phosphorylation on serines 172 and 189 (Fig. 5A, S2A, S2B) in Torin1 treated cells. However, the sequence that serines 172 and 189 lies within does not conform to the mTOR consensus phosphorylation site (Hsu et al., 2011), suggesting that phosphorylation of CAPZA^{Acp1} is TOR dependent rather than being a direct target. The Psk1 and Gad8 kinases are 2 known TORC1 and TORC2 substrates and effector kinases (Pearson and Kemp, 1991). Both Gad8 and Psk1 are members of the AGC family of kinases. However, the CAPZA^{Acp1} phosphorylation sites do not conform to the AGC kinase consensus site either. It is therefore possible that the TOR dependent CAPZA^{Acp1} phosphorylation is regulated through an as yet unidentified signalling pathway. Interestingly, serine 189 is conserved in the mammalian homologue, CAPZA (serine 208) (Fig. 5A), suggesting that TOR dependent phosphorylation of CAPZA may be conserved in metazoan systems.

TORC2 dependent phosphorylation alters CAPZA/B$^{Acp1/2}$ heterodimer formation.

The crystal structure of the human CAPZA/B heterodimer (Yamashita et al., 2003) reveals the CAPZA^{Acp1}-S189 equivalent within human CAPZA maps to the CAPZA/B interface (Fig. 5A) and therefore its phosphorylation is likely to have an impact upon heterodimer formation and function. In order to assess the impact TOR dependent CAPZA^{acp1} phosphorylation had upon CAPZA/B$^{Acp1/2}$ heterodimer formation we undertook equivalent co-immunoprecipation assays in wild type cells treated with either Torin1, to inhibit TOR signalling (Atkin et al., 2014), or DMSO. While CAPZA^{Acp1}-HA was seen to co-purify with CAPZB^{Acp2}-GFP in wild type cells, this interaction was significantly enhanced by treatment with Torin1 (Fig. 5B). A conserved mutation within the ATP-binding pocket of genes encoding for either of the two fission yeast Tor kinases specifically confers TORC1 (tor2.G2040D - TORC1^{R}) or TORC2 (tor1.G2037D- TORC2^{R}) dependent resistance to Torin1 induced inhibition (Atkin et al., 2014). These mutants can be used to establish whether Torin1 induced effects are brought about by off-target effects. Torin1 enhanced CAPZA/B$^{Acp1/2}$ heterodimer formation in wt and the TORC1^{R} mutant (Fig. 5C). In contrast, heterodimer formation was not enhanced in the TORC2^{R} mutant upon Torin1 treatment. Therefore as TORC2 activity in the TORC2^{R} mutant is resistant to the effects of Torin1, this result indicates that it is the specific inhibition of TORC2 that enhances the affinity between CAPZA^{Acp1} and CAPZB^{Acp2}.

To establish whether TORC2 dependent CAPZA^{Acp1} phosphorylation alters the stability of the CAPZA/B$^{Acp1/2}$ heterodimer we generated strains in which the endogenous CAPZA^{acp1+} locus was mutated to encode for CAPZA^{Acp1} protein in which serine 172 and 189 had been replaced with alanine to mimic an unphosphorylated serine (CAPZA^{acp1}-AA). CAPZA/B$^{Acp1/2}$ co-immunoprecipitations were repeated using extracts from CAPZA^{acp1}-AA cells and the CAPZA^{acp1}-AA mutant protein was seen to have an increased affinity for CAPZB^{Acp2} compared to wild type (Fig. 5D). Critically the Torin1 induced stabilisation of the CAPZA/B$^{Acp1/2}$ heterodimer was abolished in the CAPZA^{acp1}-AA allele (Fig. 5E). Thus these data indicate that TORC2 dependent phosphorylated of CAPZA^{Acp1} serines 172 and 189 regulates CAPZA/B$^{Acp1/2}$ heterodimer formation.

The CAPZA^{acp1}-AA/ CAPZB^{acp2} complex stabilised cortical actin polymers

The fission yeast CAPZA/B$^{Acp1/2}$ complex regulates actin dynamics and cytokinesis (Kovar et al., 2005; Nakano and Mabuchi, 2006), and recruits to the cell equator during cell division. (Movie 7). CAPZA^{Acp1}-GFP remained localised at the cell equator at the end of cytokinesis for significantly longer in Rictor$^{ste20}\Delta$ and myp2Δ cells than wild type (Fig 6A). In

contrast, the timing of RICTOR$^{Ste20\text{-}3GFP}$ CAR recruitment was unaffected in cells lacking the CAPZA^{acp1} gene (Fig 6A).

We next used Lifeact (Huang et al., 2012; Riedl et al., 2008) to compare actin dynamics in CAPZA^{acp1+} and CAPZA^{acp1}-AA mutant cells. Interestingly, the CAPZA^{acp1}-AA allele, which stabilises the CAPZA/B complex (Fig. 5D), had a significant impact upon the stability of cortical filamentous actin patches (Fig. 6B-D). Actin patches were depolarised, had a longer lifetime, and increased polymerisation rates in CAPZA^{acp1}-AA cells when compared to wild type (growth rates: wt: 220.1 AUsec^{-1}; CAPZA^{acp1}-AA: 573.8 AUsec^{-1}; shrinkage rates: wt: -167.5AUsec^{-1}; CAPZA^{acp1}-AA: -543.9 AUsec^{-1}) (Fig. S3C). Cells possessing the CAPZA^{acp1}-AA allele had 5 times more Lifeact signal associated with cortical actin patches compared to wild type (Figure 6B-D; S3C). In contrast there was no significant difference in the number of cortical actin patches, patch associated CAPZA^{Acp1} protein localised, or total CAPZA^{Acp1} protein within wild type and mutant cells (Figure S3C). This indicates the CAPZA^{acp1}-AA allele does not affect actin nucleation or stability of the CAPZA^{Acp1} protein, but remains associated with actin polymers longer than wild type which continue to accumulate actin at the uncapped end.

CAPZA^{acp1}-AA has aberrant CAR morphology

It has been suggested that cells possess a finite pool of actin monomers, for which different actin nucleators (Arp2/3 and formins) compete (Burke et al., 2014; Suarez et al., 2015). Thus increasing the proportion of the actin pool incorporated within Arp2/3 nucleated cortical actin patches would result in a reduction in the actin available for incorporation into formin nucleated actin cables, which are essential for cytokinesis to occur. CAR associated Tropomyosin^{Cdc8} provides a specific measure of formin nucleated actin cables (Skoumpla et al, 2007; Skau and Kovar, 2010). Consistent with this “finite pool of actin monomers” model quantification of the CAR associated Tropomyosin^{Cdc8} revealed a reduction in the amount of actin incorporated into Formin^{Cdc12} nucleated actin-cables within the CAR in CAPZA^{acp1}-AA cells (Fig. 6E). Therefore, while cortical actin patches are more stable and persist for longer in the CAPZA^{acp1}-AA cells, there are fewer Tropomyosin^{Cdc8} associated actin cables in the CAR. This may provide an explanation for the CAR instability in CAPZA^{acp1}-AA cells (Fig. 7A). Thus the aberrant CAR morphology phenotype observed in CAPZA^{acp1}-AA mutant cells emulates that seen in TORC2 □deletion strains. Finally, in contrast to wild type cells (Huang et al., 2012), and similar to CAPZA^{acp1}-AA the actin cytoskeleton was depolarised in Rictor$^{ste20\Delta}$ cells (Fig. 7B). This finding is consistent with the observed increased cell diameter of cells lacking TORC2 function (Fig. 1B), as cell growth may no

longer be exclusively restricted to cell ends.

Finally, stress of wild type cells at 37℃ transiently disrupts actin organisation and dynamics, before a normal distribution is re-established and growth resumes within 90 minutes (Petersen and Hagan, 2005). TORC2 has a critical role in responding to induced heat stress as TORC2 deficient cells are hypersensitive to transient increases in heat (Kawai et al., 2001; Weisman and Choder, 2001). Intriguingly, CAPZA^{acp1}-AA cells also failed to recover from the stress imposed by a shift from 28℃ to 37℃ (Fig. 7C). CAPZA^{Acp1} protein levels did not change following heat stress of either wild type or CAPZA^{acp1}-AA cells (Fig S3A). Hence the mutations did not affect CAPZA^{Acp1} stability, and the alteration in actin dynamics may cause the observed increased sensitivity to heat stress in CAPZA^{acp1}-AA cells.

In summary, we conclude that TORC2 dependent phosphorylation of CAPZA^{Acp1} reduces the stability of the CAPZA/B$^{Acp1/2}$ heterodimer. This in turn modulates the stability of cortical actin patches and alters the concentration of free monomeric-actin within the cell, to affect the timing and fidelity of cytokinesis.

Discussion

Here we describe a novel TORC2 recruitment to the Cytokinetic Actomyosin Ring (CAR) that plays a role in maintaining the fidelity of cytokinesis in fission yeast. We describe a mechanism by which a myosin V and myosin II co-purify with TORC2 and play a role in its localisation to the CAR during cytokinesis. Each myosin appears to play a discrete role in affecting TORC2 CAR localisation. Myo51 ensures TORC2 recruits to the CAR in the early stages of anaphase, while Myp2 maintains TORC2 at the CAR. While TORC2 is required to maintain the CAR at the cell equator and prevent it from drifting along the cell cortex, both TORC2 and Myp2 maintain the integrity of a single CAR structure and prevent it from splitting in two during its constriction. It is currently unclear why RICTOR^{ste20} only associates with the CAR in a subset of *myp2*Δ cells, however this may explain why a cytokinesis defects is only observed in a subset of cells lacking this myosin II.

In the absence of TORC2 signalling the stability and activity of the actomyosin ring and therefore cytokinesis are altered. These changes in actin dynamics arise in part from TORC2 dependent phosphorylation of the actin capping protein CAPZA^{Acp1}. Perturbation of CAPZA^{Acp1} phosphorylation increases the stability of the CAPZA/B$^{Acp1/2}$ heterodimer (Fig. 5), it significantly alters the cellular organisation of the actin cytoskeleton (Fig. 6), and it disrupt CAR function (Fig. 7A). The increased severity in growth and cytokinesis phenotypes of RICTOR^{ste20}*Δ* cells compared to the CAPZA^{acp1}-AA and myp2*Δ* mutants (Fig. 1, 3 & 7) suggest that CAPZA^{acp1} is very unlikely to be the sole protein with a key role in cytokinesis that is regulated in a TORC2 dependent manner. Consistent with this view an increase in myosin II Myo2 levels was seen in the RICTOR^{ste20}*Δ* cells but not in acp1*Δ* or myp2*Δ* (data not shown), thus TORC2 regulate Myo2 in an yet unidentified manner. Multiple potential TORC2 regulated proteins involved in coordinating cell division, co-purified with TORC2 (Fig. 2A). However, our SILAC analysis to date has not identified phospho-peptides that showed differential phosphorylation upon Torin1 inhibition of TOR function in any of the co-purifying proteins. Critically, we recently demonstrated that the co-purifying SCYL family pseudo-kinase Ppk32 is a novel regulator of TOR signalling; and intriguingly Ppk32 concentrates at the cell equator during cell division in more than 60% of cells (Kowalczyk and Petersen, 2016). Thus, the TORC2 dependent regulation of CAPZA/B$^{Acp1/2}$ that we describe here is likely to be one of multiple TORC2 dependent mechanisms regulating the fidelity and timing of cytokinesis and cell division.

The TORC2 control of CAPZA/B$^{Acp1/2}$ heterodimer stabilisation enables cells to couple actin stability with changes in cell growth and division, which can be implemented in

response to environmental stress. Crucially, this TORC2 dependent change in CAPZA/B$^{Acp1/2}$ affinity and actin stability provides an explanation for the enhanced F-actin cable stability observed in TORC2 deficient cells (Ikai et al., 2011; Matsuo et al., 2007), which appears to be key in ensuring cell survival following environmental stress. Similar controls are likely to underlie TORC2 control of actin dynamics and cytokinesis in mammalian cells, as knockout of TORC2 components in HeLa cells leads to similar increases in the abundance of actin fibres and increased cytoplasmic paxilin association (Sarbassov et al., 2004). Furthermore, serine 2481 auto-phosphorylated mTOR localises to the cleavage furrow at the onset of cytokinesis (Vazquez-Martin et al., 2009) suggesting that active mTOR plays a conserved role in cytokinesis and cell division.

Acknowledgements

We thank Kazuhiro Shiozaki, David Kovar and Iain Hagan for reagents; Iain Hagan and members of the laboratories for stimulating discussions and valuable comments on the manuscript. We thank the Biological Mass Spectrometry Facility at university of Manchester for protein identification. This work was supported by the Universities of Kent, Manchester and Flinders and funding from the Biotechnology and Biological Sciences Research Council (BB/J012793/1) and a Royal Society Industry Fellowship to D. Mulvihill; a CASE industrial bursary from Cairn Research Ltd to KB; Two Wellcome Trust funded studentships to JA and DC and a Cancer Research UK Senior Fellowship to J. Petersen [grant number C10888/A11178]

Material and Methods

Strains and cell cultures.

Strains used in this study are listed in Supplementary Table S1. Unless otherwise specified, cells were cultured at 28ºC in Edinburgh minimal media (EMM2) (Fantes, 1977) using 20 mM L-Glutamic acid as a nitrogen source (EMMG). Cells were grown exponentially for 48hr before being harvested or examined microscopically at early exponential phase of 1.5 x 10^6 cells/ml. Rictor$^{ste20\Delta}$ cells frozen immediately after spore germination. Cells were tested for sensitivity to stress and sterility to insure no suppressors had accumulated. All Rictor$^{ste20\Delta}$ cells cultures were maintained in exponential growth and never exposed to starvation.

FACS analysis.

S. pombe DNA content were measured by flow cytometry as previously described (Costello et al, 1986).

Large scale Tor1 immunoprecipitation (IP).

Wild type cells (JP350) were grown in EMMG to 2.5×10^6 cells/ml (5 litres per IP condition) harvested and disrupted using a freezer mill (SPEX 6870) in liquid nitrogen. The cell powder was thawed with IP buffer (50 mM HEPES pH 7.5, 150 mM NaCl, 0.1% CHAPS, 50mM L-arginine, 50mM L-glutamic acid, 0.05% Tween 20, 120 mM β-glycerophosphate di-sodium salt, 4mM Na_3VO_4, 100 mM NaF, 2 mM PMSF, 10mM N-ethylmaleimide, 2mM dithiothreitol and 2 x Roche EDTA free protease inhibitor cocktail). The cleared supernatant was incubated with Invitrogen protein G Dynabeads, pre-incubated with anti-tor1 antibodies or PK (V5) (AdB Serotec) antibody for control, for 60 min at 4℃. Beads were then washed twice with IP buffer plus 50mM NaCl (200mM final concentration) proteins were eluted by heating at 80℃ for 10 min. The samples were loaded on a NUPAGE Bis-Tris 4–12% gel (Life Technologies). The gel was fixed with 7% acetic acid and 25% methanol and stained by Brilliant blue. The entire lane was cut into small bands, before being sent for protein identification. Mass spectrometry data were analysed by Scaffold^{TM} 3 software.

Immunoprecipitation of Myo51 cargo binding domain

Immunoprecipitation and cell lysis was performed in the following buffer – 50mM HEPES pH7.5, 150mM NaCl, 0.1% CHAPS, 50mM L-arginine, 50mM L-glutamic acid, 0.05% Tween, 50mM NaF, 2mM Na_3VO_4, 60mM β-glycerophosphate di-sodium salt, 5mM N-ethylmaleimide, 1mM PMSF, 10μM Z-LLF 1mM DTT and 1x protease inhibitor without EDTA (Complete, Mini - Roche), with the addition of 150mM NaCl (300mM final

concentration) and 100mM KCl for washes. 6 x10^8 cells, harvested at a density of 2x10^6/ml, were used per IP. Protein A dynal beads (Life Technologies) were used and the cell lysis solution was pre-cleared for 10 mins with a bead only slurry. Cleared extracts were incubated with GFP monoclonal antibody (clones 7.1 and 13.1 - Roche) pre-coated dynal A beads for 30min at 4℃ and washed 5 times prior to elution from beads in loading buffer at 70℃ for 15mins.

SILAC cell culture.

car2::NAT lys1-131 arg3-d4 cells were inoculated in YES media overnight and then washed into EMM-G containing 75mg/L of either light (l-arginine monohydrochloride (Sigma) and l-lysine monohydrochloride (Sigma)) or medium ((LYSINE-L, 2HCl 4.4.5.5-D4 (Cat code DLM-2640, Euroisotop), ARGININE-L, HCl, U-13C6 99%13C (Cat code CLM-2265, Eurisotop,)) amino acids. Cells were cultured in log phase for 48 hours to ensure complete incorporation of labelled amino acids into the proteome. Light labelled cultures were treated with DMSO and medium labelled cultures were treated with a final concentration of 25 µM Torin1 at a density of 2.04 x 10^6 cells/ml. Approximately 4.8 x 10^9 cells were harvested for each sample. After 30 minutes cultures were harvested by centrifugation, washed in 20ml of STOP buffer (10 mM EDTA, 1 mM sodium azide, 50 mM sodium fluoride (NaF), 0.9% NaCl), followed by washing with 10ml of ice cold dd$H_2$0. The final pellets were then resuspended in an appropriate volume of ice cold dd$H_2$0 and dropped directly into liquid nitrogen to produce frozen cell droplets.

SILAC Protein extraction.

Samples were processed using a SPEX Sample Prep LLC 6850 Freezer Mill in presence of liquid nitrogen. The resulting cell powder was resuspended in denaturation buffer (6M urea, 2M thiourea, 1% n-octyl glucoside) at a ratio of 500mg powder to 500µl denaturation buffer. Insoluble material was removed by centrifugation (13,000 g, 10 minutes at 4℃) and the supernatant was designated supernatant I (soluble fraction). The pellet was then resuspended in 500µl denaturation buffer, 500µl glass beads were added and then subjected to 20 seconds shaking in a FastPrep machine (FP120, Qbiogene). The resulting suspension was again centrifuged (13,000 g, 10 minutes at 4℃) and the supernatant retained (supernatant II). The pellet was then discarded. Protein concentrations were determined by Bradford assay according to manufacturers instructions.

Mass spectrometry for SILAC.

Respective supernatants I and II derived from the “light” and “medium” labelled cell cultures were combined and proteins were precipitated at -20℃ using ice-cold acetone /methanol left on ice overnight. The proteins were pelleted by centrifugation (2200 x g, 20 min, 4℃) and washed with 80% ice-cold acetone. Dried proteins were resolved in digestion buffer (6 M urea, 2 M thiourea, 10 mM Tris, pH 8.0) and mixed in 1:1 ratio according to measured protein amounts. The mixtures were digested in solution with trypsin as described previously (Borchert et al., 2010). For proteome analyses 100µg of the mixtures were fractionated by isoelectric focusing on an OffGel 3100 Fractionator (Agilent) according to the manufacturer’s instructions. Focusing was performed using with 13 cm (12 well) Immobiline DryStrips pH 3–10 (Bio-Rad) at a maximum current of 50 µA for 24 kVh. Peptide fractions were collected and desalted separately using C18 StageTips (Rappsilber et al., 2007).

For phosphoproteome analyses eight milligrams of each peptide mixture was subjected to phosphopeptide enrichment as described previously (Olsen et al., 2005) with minor modifications: Peptides were separated by strong cation-exchange (SCX) chromatography with a gradient of 0 to 35% SCX solvent B resulting in seven fractions that were subjected to phosphopeptide enrichment by TiO_2 beads. Elution from the beads was performed three times with 100 µl of 40% ammonia hydroxide solution in 60% acetonitrile (pH > 10.5). Fractions rich in peptides were subjected to multiple TiO2 enrichment. Enrichment of phosphopeptides from the SCX flow-through was completed in five cycles.
LC-MS/MS analyses were performed on an EasyLC nano-HPLC (Proxeon Biosystems) coupled to an LTQ Orbitrap XL (Thermo Scientific) for phosphopeptide analyses, or an LTQ Orbitrap Elite mass spectrometer (Thermo Scientific) for proteome analyses as described previously (Koch et al., 2011). The peptide mixtures were injected onto the column in HPLC solvent A (0.5% acetic acid) at a flow rate of 500 nl/min and subsequently eluted with a 87-min (proteome) or a 127-min (phosphoproteome) segmented gradient of 5–33-90% HPLC solvent B (80% ACN in 0.5% acetic acid). During peptide elution the flow rate was kept constant at 200 nl/min. For proteome analysis the twenty most intense precursor ions were sequentially fragmented in each scan cycle. For the phosphoproteome analysis the five most intense precursor ions were fragmented by multistage activation of neutral loss ions at -98, -49, and -32.6 Th relative to the precursor ion (Schroeder et al., 2004). In all measurements, sequenced precursor masses were excluded from further selection for 90 s. Full scans were acquired at resolution of 60,000 (Orbitrap XL), or 120,000 (Orbitrap

Elite). The target values were set to 5000 charges for the LTQ (MS/MS) and 10^6 charges for the Orbitrap (MS), respectively; maximum allowed fill times were 150ms (LTQ) and 1000 ms (Orbitrap). The lock mass option was used for real time recalibration of MS spectra (Olsen et al., 2005).

The MS data of all SILAC experiments were processed using default parameters of the MaxQuant software (v1.2.2.9) (Cox and Mann, 2008). Extracted peak lists were submitted to database search using the Andromeda search engine (Cox et al., 2011) to query a target-decoy (Elias and Gygi, 2007) database of S. pombe proteome (http://www.pombase.org/, Protein Dataset in FASTA format, downloaded on the 6th of April 2011), containing 5076 protein entries and 248 commonly observed contaminants.

Molecular manipulations and generation of single point mutations.

The CAPZA$^{acp1\Delta}$ base strain: A DNA cassette for acp1 deletion was prepared by PCR amplification. This construct was used to replace the acp1$^+$ gene at the native locus with the nat$^+$. To generate the acp1-S172A-S189A point mutations, standard site directed mutagenesis. The mutant acp1 was then used to replace the nat1 rpl42$^+$ gene in JP2222 (Fennessy et al., 2014). The resulting strains were back-crossed and prototroph progeny was selected. The presence of the acp1 S/A allele was verified by PCR. Thus all acp1 single point mutations used in this study are integrated into the acp1 locus, and are all prototroph strains. C-terminal tagging method as previously (Bahler et al., 1998) using acp1 C-terminal specific primers

Acp1-HA immunoprecipitations

Immunoprecipiation of Acp1-HA was carried out under non-denaturing conditions allowing for pull down of any bound Acp2-GFP. Cell lysis buffer consisted of 50mM HEPES pH7.5, 100mM KCl, 50mM NaCl, 0.2% Tween, 0.1mM EDTA, 1x protease inhibitors (Complete, Mini - Roche), 25mM NaF, 2mM Na_3VO_4, 25mM β-glycerophosphate di-sodium salt, 5mM N-ethylmaleimide, 0.5mM PMSF, with the addition of a further 25mM NaCl and 0.25% CHAPS in wash buffer. Briefly, HA antibody (F7 clone - Santa Cruz Biotechnology) was dimethyl pimelimidate cross-linked to Dynal beads protein A (Life Technologies) and incubated with lysed S. pombe cells ($3x10^8$ cells per IP, harvested at $1.5x10^6$cells/ml) for one hour at 4℃, followed by 5 x washes with wash buffer. Boun d proteins were eluted in loading buffer (100mM TrisHCl pH6.8, 4% SDS, 0.2% bromophenol blue, 20% glycerol, 100mM DTT) at 70℃ for 15 mins then loaded onto 12% tris-glycine PAGE, transferred to

PVDF membrane and the membrane cut at approximately 45kDa enabling detection of both CAPZA^{Acp1}-HA and CAPZB^{Acp2}-GFP on the same gel.

Western blotting.

TCA precipitation protocol was followed for total protein extracts (Caspari et al., 2000). The following dilutions of antibodies were used in this study. 1/1000 anti-Myo2 (Coulton et al., 2010) (1/100 anti-GFP (Source), anti-HA (F7). Alkaline phosphatase coupled secondary antibodies were used for all blots followed by direct detection with NBT/BCIP (VWR) substrates on PVDF membranes.

Microscopy: Samples were visualised using an Olympus IX71 microscope with PlanApo 100x OTIRFM-SP 1.45 NA lens mounted on a PIFOC z-axis focus drive (Physik Instrumente, Karlsruhe, Germany), and illuminated using LED light sources (Cairn Research Ltd, Faversham, UK) with appropriate filters (Chroma, Bellows Falls, VT). An Optosplit device (Cairn Research Ltd) was used to allow simultaneous acquisition of signals from two fluorophores that emitted light of different wavelengths. Samples were visualised using either a QuantEM (Photometrics) or ProEM 1024B (Princeton Instruments) EMCCD camera, and the system was controlled with Metamorph software (Molecular Devices). Each 3D-maximum projection of volume data was calculated from 21 z-plane images, each 0.2 µm apart, and analysed using Metamorph and Autoquant X software. During live-cell imaging, cells were cultured in Edinburgh minimal media using 20 mM L-Glutamic acid as a nitrogen source (EMMG). Cells were grown exponentially at 25ºC for 48hr before being mounted (without centrifugation) onto lectin (Sigma L2380; 1 mg/ml) coated coverslips with an a Bioptechs FCS2 (Bioptechs, Butler, PA), fitted onto an ASI motorised stage (ASI, Eugene, OR) on the above system, with the sample holder, objective lens and environmental chamber held at the required temperature. Cdc8 immunofluorescence was undertaken using conditions described previously (Skoumpla et al., 2007). Mean cell width, septa positioning, and nuclear diameter was determined from measurements of ~300 cells for each strain. In the determining the timing of CAR formation and constriction, and protein recruitment in wild type and mutant strains, time-lapse imaging and subsequently analysis was undertaken on >20 cells for each individual strain.

Figures

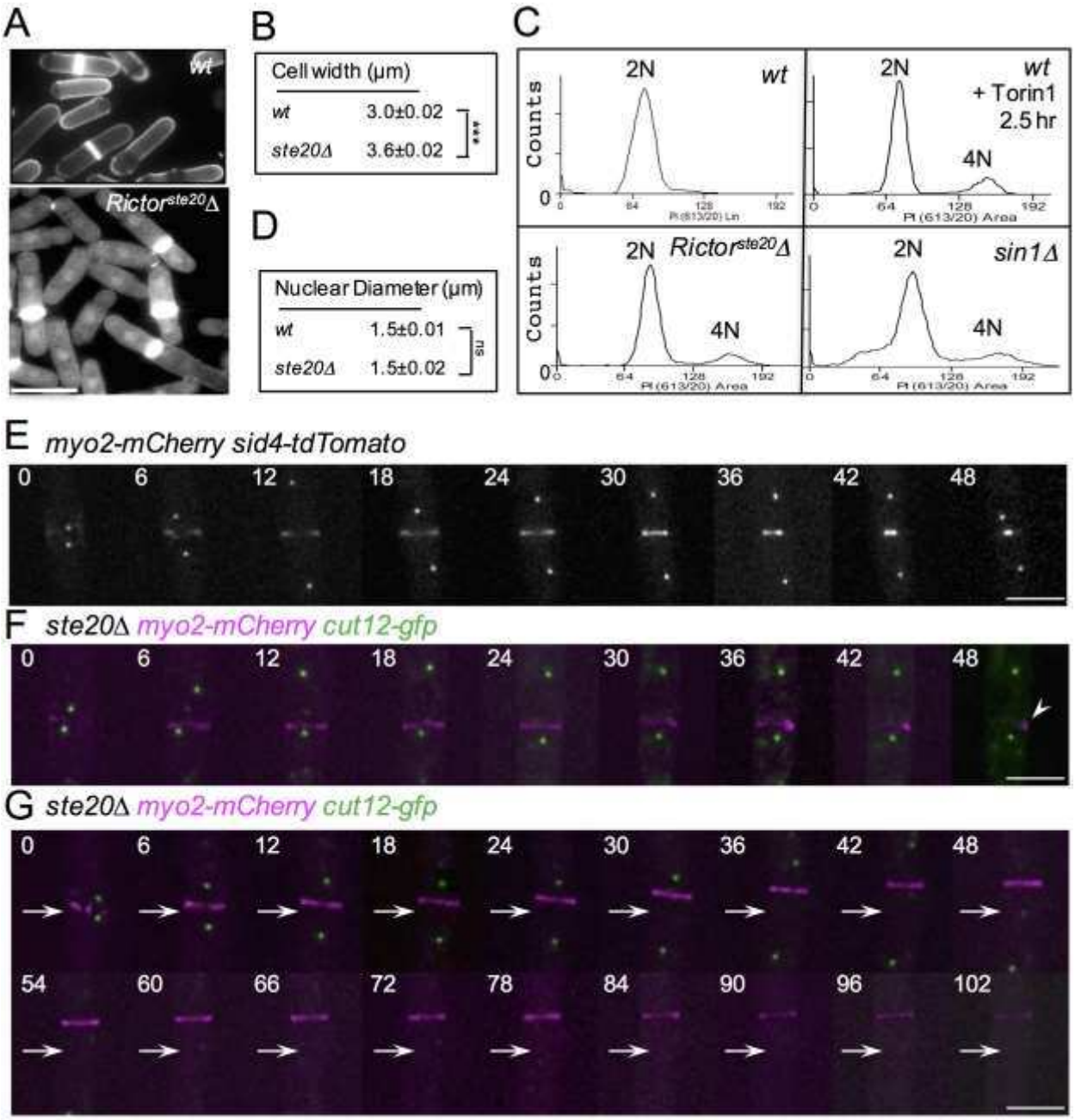

Figure 1: TORC2 deficient mutants display defects in cytokinesis and cell fission.

(A) Early exponential prototroph cells were stained with calcofluor to visualise the division septa (Scale – 10 μm), and (C) processed for flow cytometry analysis to measure DNA content. Mean cell width (B) and nuclear diameter (D) were each determined from counting 300 wt and *ste20*Δ cells in mid log culture. (E) A montage of timelapse images showing red fluorescence from myo2-mCherry sid4-tsTomato cells undergoing cell division. Cells illustrating timing of CAR formation and constriction in relation to SPB segregation in wild

type cells. (F & G) Equivalent montages of time-lapse images of mCherry (magenta) and GFP (green) fluorescene from myo2-mCherry cut12-gfp *ste20*Δ cells. In a large proportions of anaphase *ste20*Δ cells the CAR was seen to either collapse (F) or drift along the cortex toward one end of the cell (G). Scale – 5 µm.

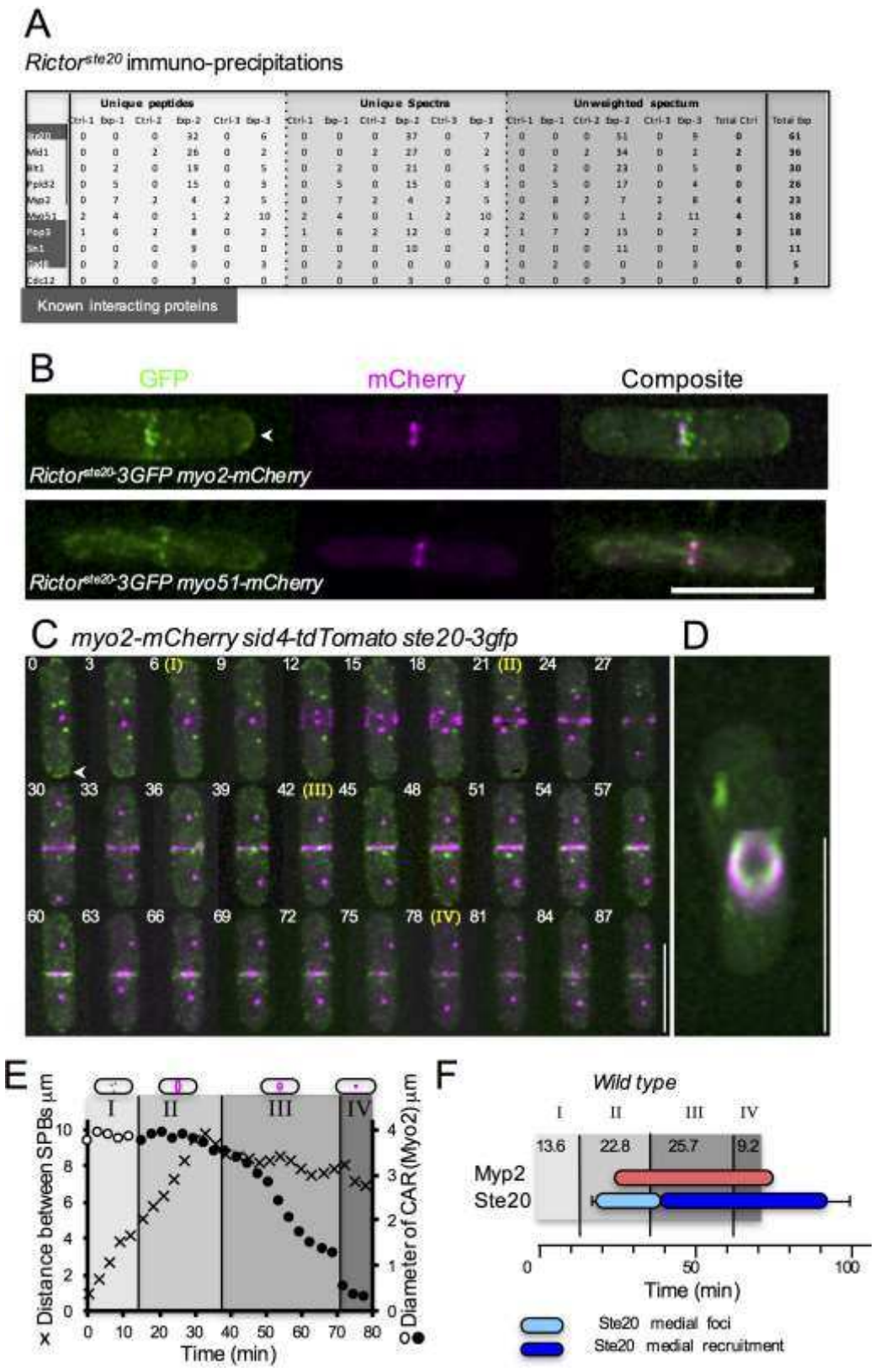

Figure 2: TORC2 interacts with and localises to the Cytokinetic Actomyosin Ring during ring constriction.

(A) Summary of mass spec analysis of 3 independent experiments of control (Ctrl – no anti-Tor1 antibodies added) and Tor1 immunoprecipitations (Exp), each purified from 20 litre cell cultures. (B) Micrographs of Rictor^{Ste20} (green) and Myo2 or Myo51 (magenta) signal from mitotic Rictor^{ste20-}GFP myo2-mCherry cells or Rictor^{ste20-}GFP myo51-mCherry cells. (C & D) Maximum projections of 21 slice z-stacks from a time course of mitotic myo2-mCherry sid4-tdTomato ste20-3gfp cells reveals Ste20 foci (green) recruits to the cell equator after SPB (magenta) separation and Myo2 ring (magenta) formation has occurred (frame 1-4 with non-separated SPBs represent interphase cells) (C) and coalesce to form a ring during CAR constriction (D). Micrograph of mCherry and GFP signal from Rictor^{ste20-}3GFP myo2-mCherry and Rictor^{ste20-}3GFP myo51-mCherry cells illustrate TORC2 association with the CAR. (E) The timing of key events during CAR formation and constriction: (I) Myo2 foci (empty circles) recruit to the cell equator; (II) Myo2 foci coalesce to form a CAR (filled circles); (III) The CAR constricts until, (IV) reaching a diameter of 0.5 µm or less) were determined in relation to nuclear division (cross: distance between SPBs) in wild type. (B - C) Arrowheads highlight RICTOR^{Ste20}localisation at cell tips. (F) The timing of Myp2 ring (red bars) and Ste20 medial foci (light blue bars) or Ste20 ring recruitment (dark blue) were determined in wild type strains in relation to the events determined in (E). Scales – 10 µm.

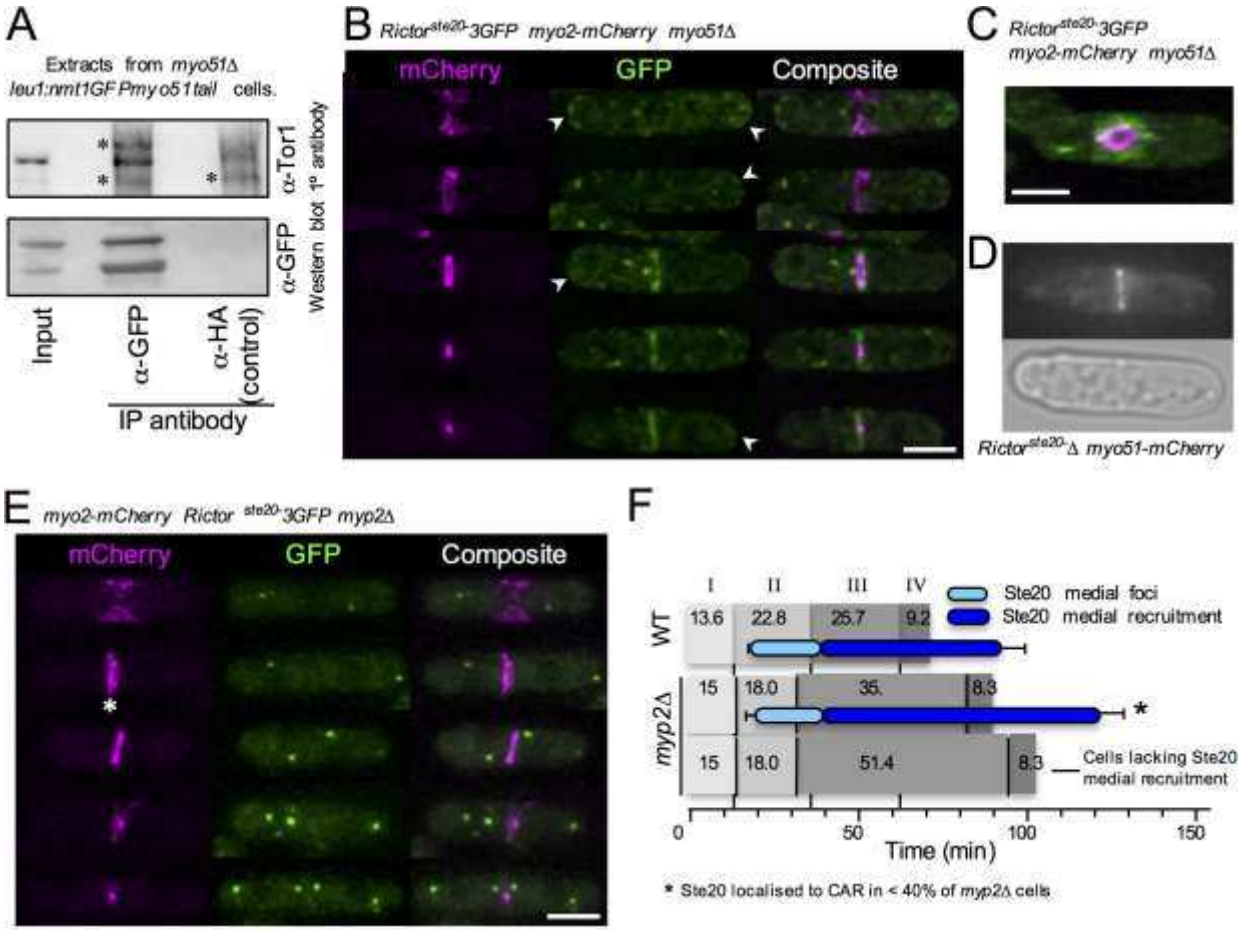

Figure 3: Myosin II & V interact with and regulate RICTOR^{Ste20} localisation at the CAR. (A) Extract and subsequent anti-GFP and anti-HA (control) immunoprecipitates from S. pombe cells expressing a GFP-tagged Myo51 Cargo-binding-tail domain fusion protein were subject to anti-Tor1 (upper panels) and anti-GFP (lower panels) western blot analysis. * denotes background bands. (B-E) Micrographs of mCherry and GFP signals in cells with the indicated genotype. Asterisk highlights rings split in two. Arrowheads highlight RICTOR^{Ste20}localisation at cell tips. (F) The timing of and Ste20 medial foci (light blue bars) or Ste20 ring recruitment (dark blue) were determined in wild type and *myp*2Δ strains in relation to the events determined in (2E). Scales - 5 µm.

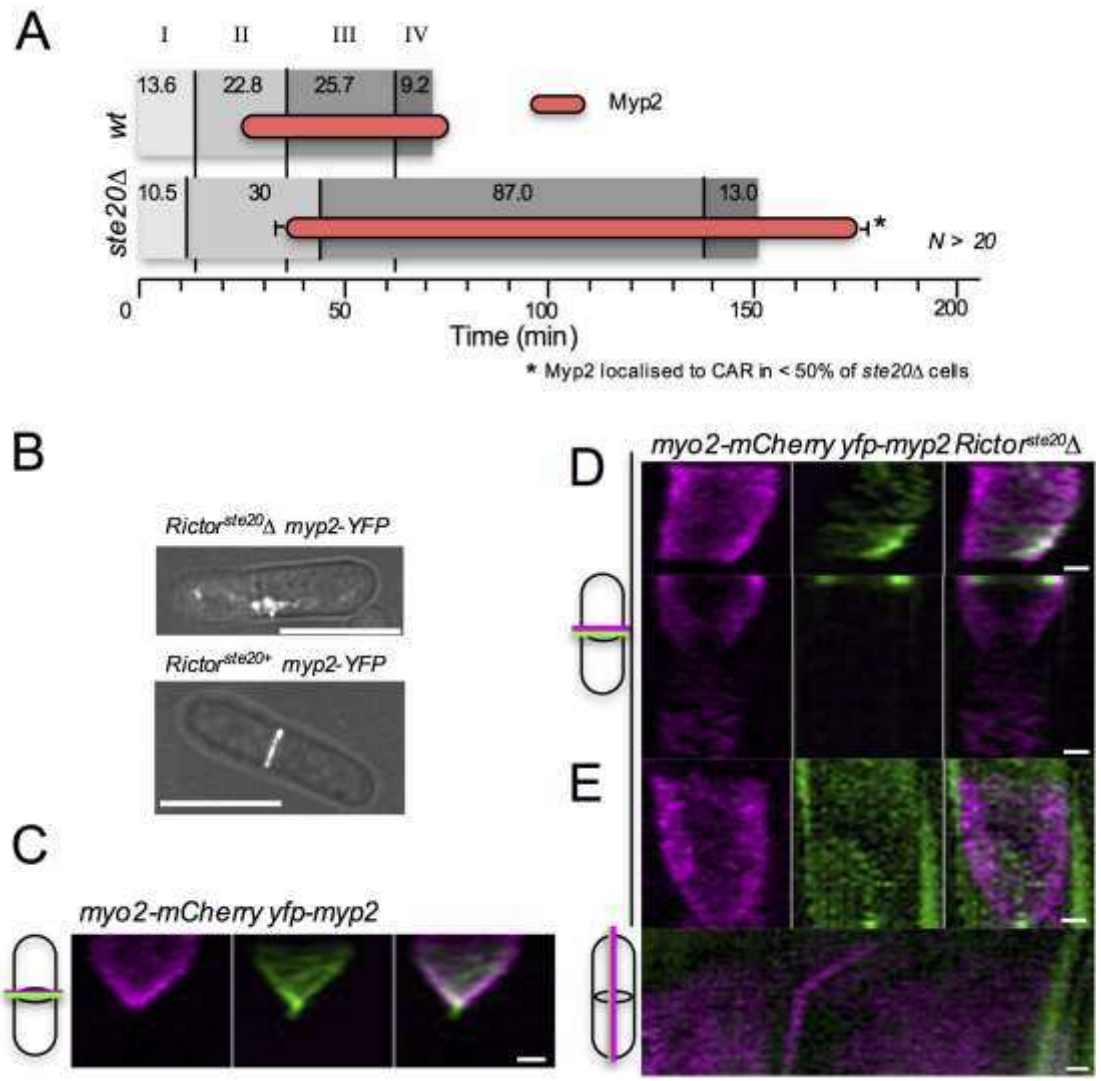

Figure 4: Myp2 and TORC2 localisation to the actomyosin ring is co-dependent.

(A) The timing of and Myp2 ring recruitment (red bars) were determined in wild type and Rictor$^{ste20}\Delta$ strains in relation to the events determined in (2E). (B) Composite micrographs of YFP and phase signal in yfp-myp2 Rictor^{ste20+} and yfp-myp2 Rictor$^{ste20}\Delta$ cells. (C-E) Kymographs generated from 30 maximum projections of timelapse images (3 min/frame) of (C) myo2-mCherry YFP-myp2 and (D) myo2-mCherry YFP-myp2 Rictor$^{ste20}\Delta$ cells illustrate TORC2 is required for Myp2 to remain at the CAR. (E) Timelapse kymographs of the perpendicular (upper panels) and longitudinal (lower panels) axes of yfp-myp2 Rictor$^{ste20}\Delta$ cell in which Myp2 signal is lost from the cell equator, and the Myo2 containing CAR slides along the cell cortex before constricting. (C-E) Cartoons illustrate orientation and origin of kymograph axes.. Scales – 5 (B) or 1 (C-E) µm.

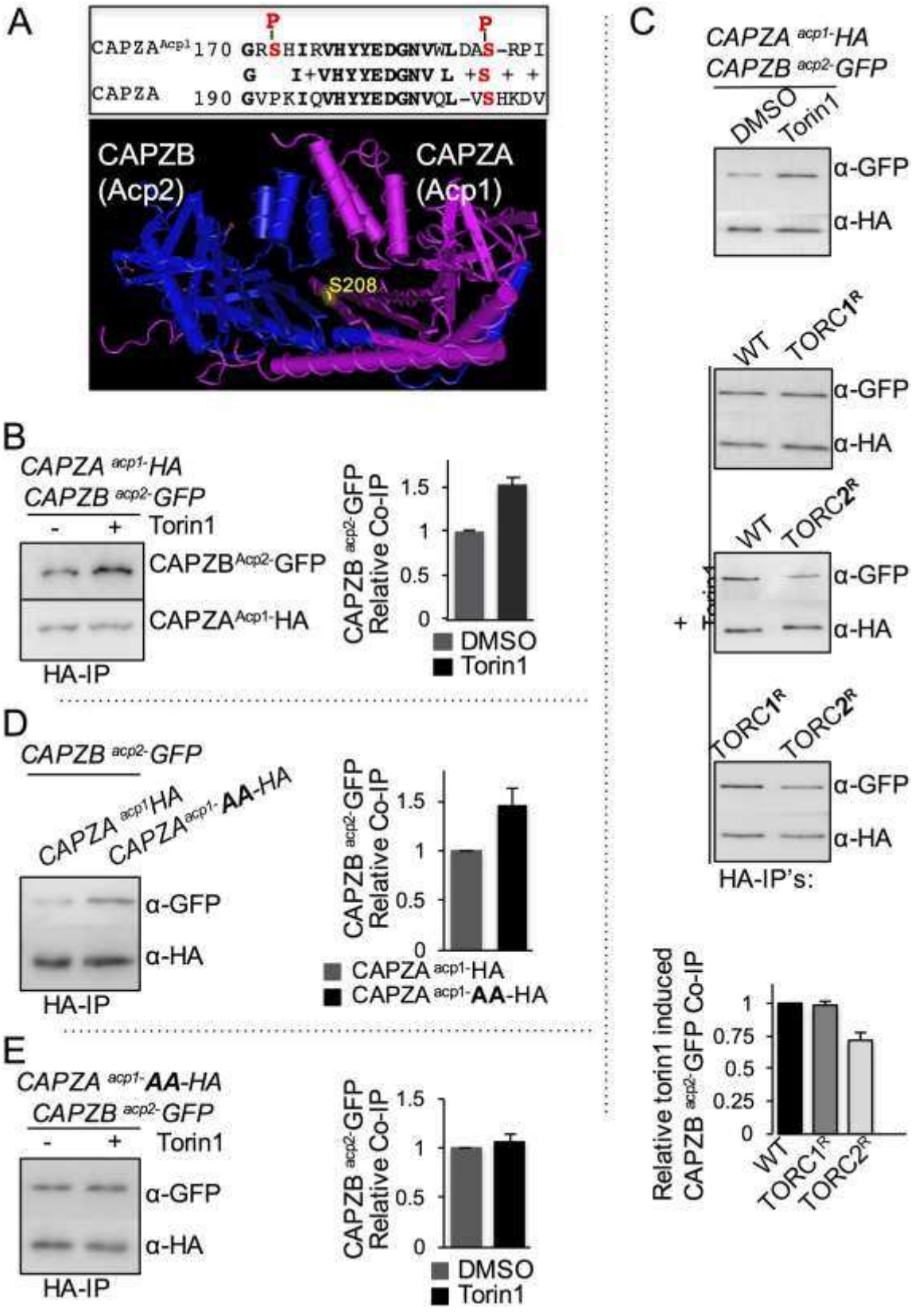

Figure 5: TORC2 regulates CAPZA/B$^{Acp1/2}$ heterodimer formation

(A) Alignment of phosphorylated region of S. pombe Acp1 and human homologue, CAPZA. Conserved residues are highlighted in bold and the two TOR dependent phosphorylation sites are shown in red. The position of the conserved phosphorylated serine 208 (in yellow) is shown on the crystal structure of CAPZA and CAPZB (Yamashita et al., 2003)**.** (B-D) Anti-GFP (upper panels) and anti-HA (lower panels) western blots of $CAPZA^{Acp1}$-HA immune-precipitations from indicated strains in the absence or presence of the TOR inhibitor Torin1 (25µM) ($TORC1^{R}$ = tor2.G2037D $TORC2^{R}$ = tor1.G2040D).

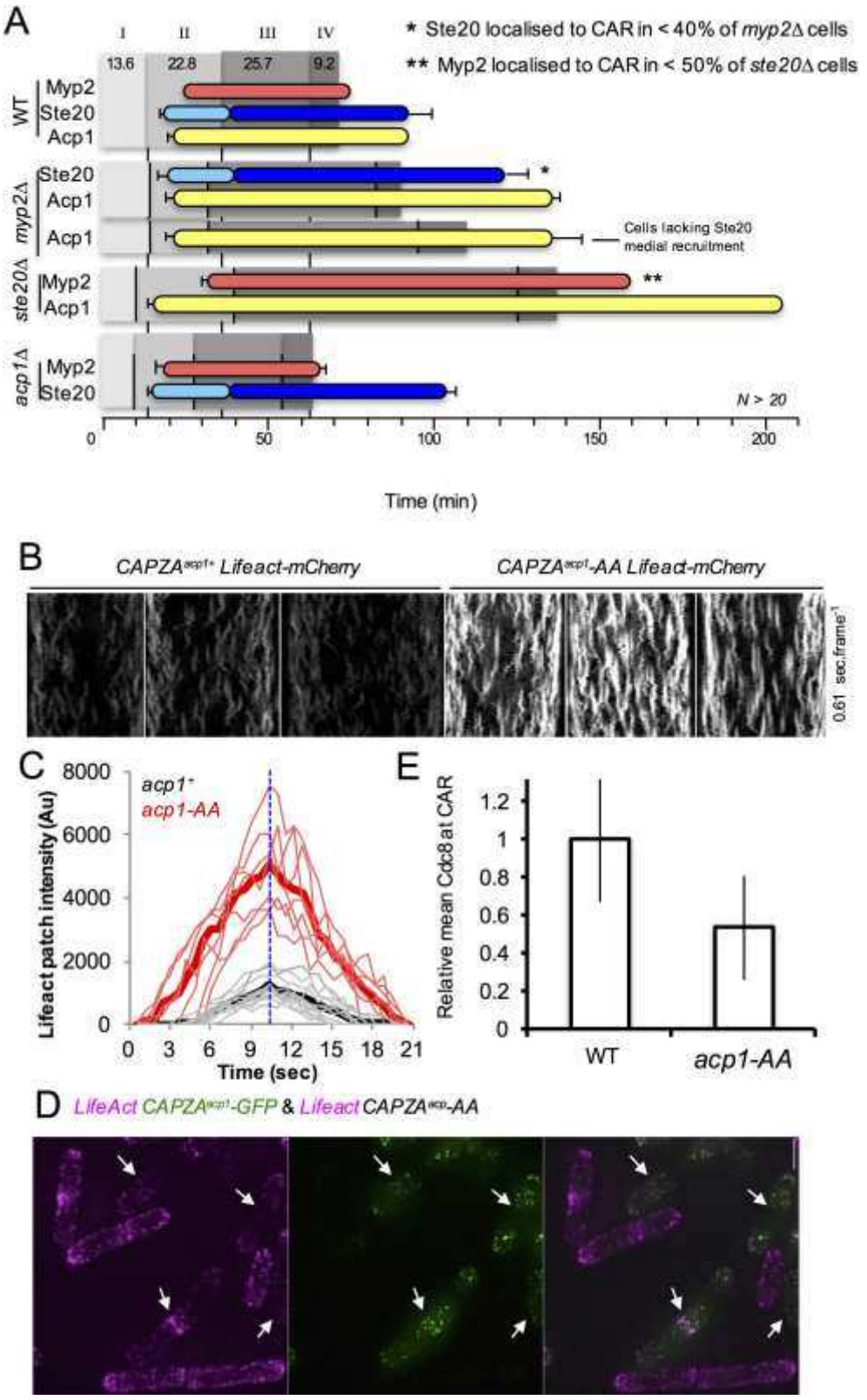

Figure 6: CAPZA^{Acp1}-AA mutants disrupt actin dynamics and cytokinesis.

(A) The timing of Myp2 ring (red bars), Ste20 foci (light blue bars) , Acp1 (yellow bars) medial recruitment and Ste20 ring recruitment (dark blue) were determined in wild type, *myp2*Δ, *ste20*Δ and *acp1*Δ strains in relation to the events determined in (Fig. 2E). * - Recruitment of these proteins to the CAR were observed in less than 50% of the deletion strains. CAR dynamics and composition were followed in >20 cells for each strain. Early exponential prototrophs were used in each experiment. (B) mCherry kymographs generated from 100 timeframe maximum projections from 13 z-plane images of CAPZA^{acp1+} Lifeact-mCherry (left panels) and CAPZA^{acp1}-AA Lifeact-mCherry (right panels) cells (0.6 sec/frame). (C) Graph showing lifetime kinetics of Lifeact signal from individual (faint lines) actin patches and overall averages (thick lines) of CAPZA^{acp1+} Lifeact-mCherry (black lines) and CAPZA^{acp1}-AA Lifeact-mCherry (red lines) cells. (D) Maximum projections of a mixture of CAPZA^{acp1}-GFP Lifeact-mCherry and CAPZA^{acp1}-AA Lifeact-mCherry cells. Overlaying the GFP (green) and mCherry (magenta) signals demonstrate the increase in actin signal at cortical actin patches in the CAPZA^{acp1}-AA mutant compared to GFP labelled wild type (arrows) cells. (E) Histograms illustrating mean relative Tropomyosin^{Cdc8} at the CAR in wtand CAPZA^{acp1}-AA cells (n>30 / strain).

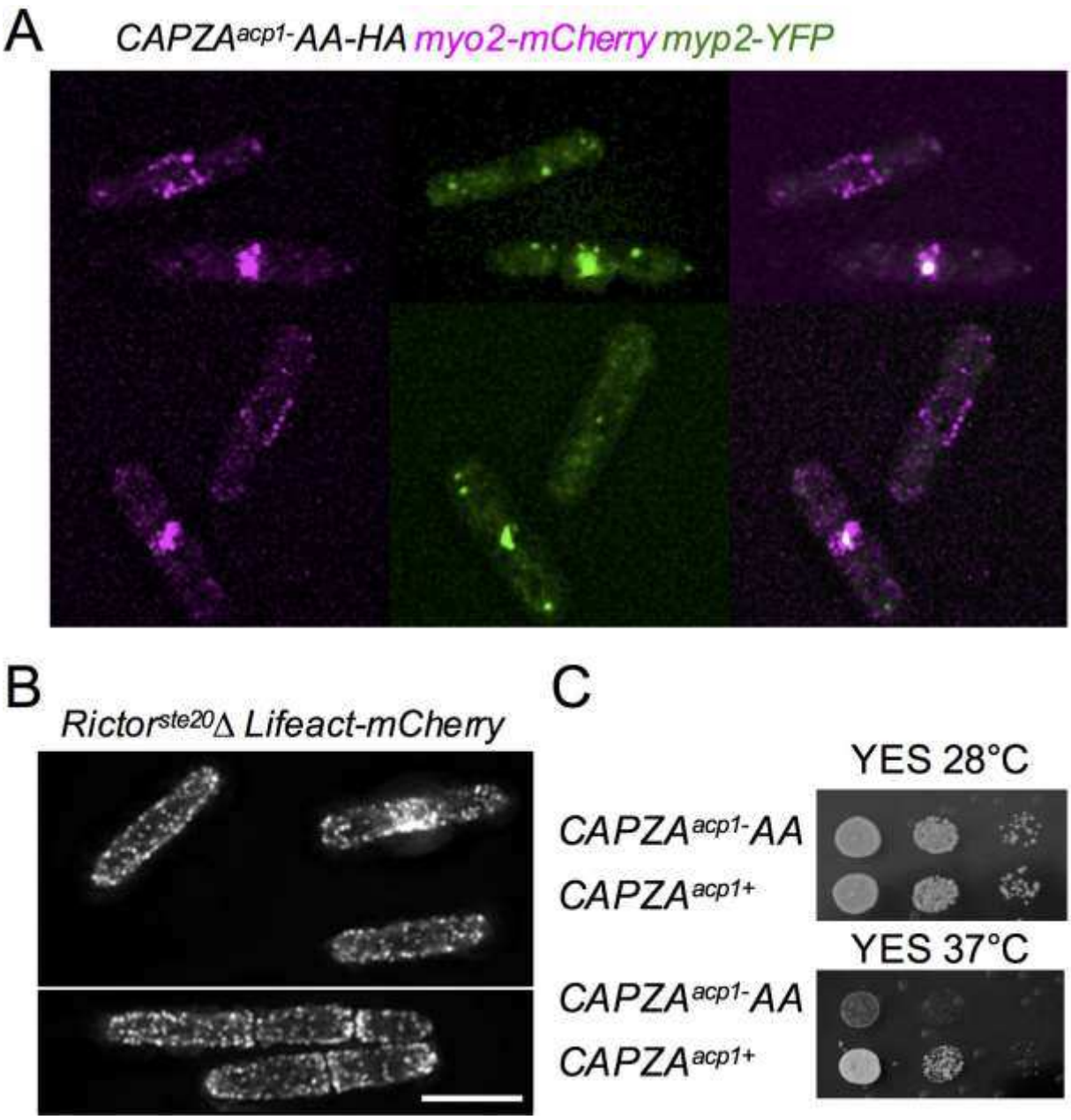

Figure 7: TORC2 and CAPZA^{Acp1}-AA mutants disrupt CAR and actin localisation.

(A) Micrographs of Myo2 (magenta) and YFP (green) signal from CAPZA^{acp1}-AA-HA myo2-mCherry YFP-myp2 cells. (B) Micrograph of mCherry signal from Rictor$^{ste20\Delta}$ Lifeact-mCherry cells illustrate cytokinesis defect and lack of polarised actin signal. (C) The CAPZA^{acp1} phosphorylation site mutant CAPZA^{acp1}-AA is sensitive to heat stress at 37℃.Model: TORC2 localises to the actomyosin ring during cytokinesis. The affinity of actin capping protein CAPZA^{Acp1} to CAPZB^{Acp2} is regulated in a TOR dependent way and it is critical for regulating actin and CAR dynamics. Scales - 10 μm.

References

Alvarez, B. and Moreno, S. 2006. Fission yeast Tor2 promotes cell growth and represses cell differentiation. J Cell Sci. 119:4475-4485.

Atkin, J., Halova, L., Ferguson, J., Hitchin, J.R., Lichawska-Cieslar, A., Jordan, A.M., Pines, J., Wellbrock, C. and Petersen, J. 2014. Torin1-mediated TOR kinase inhibition reduces Wee1 levels and advances mitotic commitment in fission yeast and HeLa cells. J Cell Sci. 127:1346-1356.

Bahler, J., J.Q. Wu, M.S. Longtine, N.G. Shah, A. McKenzie, A.B. Steever, A. Wach, P. Philippsen, and J.R. Pringle. 1998. Heterologous modules for efficient and versatile PCR-based gene targeting in Schizosaccharomyces pombe. Yeast. 14:943-951.

Bezanilla, M., S.L. Forsburg, and T.D. Pollard. 1997. Identification of a second myosin-II in Schizosaccharomyces pombe: Myp2p is conditionally required for cytokinesis. Molecular Biology Of the Cell. 8:2693-2705.

Bimbo, A., Y. Jia, S.L. Poh, R.K. Karuturi, N. den Elzen, X. Peng, L. Zheng, M. O'Connell, E.T. Liu, M.K. Balasubramanian, and J. Liu. 2005. Systematic deletion analysis of fission yeast protein kinases. Eukaryotic cell. 4:799-813.

Borchert, N., C. Dieterich, K. Krug, W. Schutz, S. Jung, A. Nordheim, R.J. Sommer and B. Macek. 2010. Proteogenomics of Pristionchus pacificus reveals distinct proteome structure of nematode models. Genome research. 20:837-846.

Burke, T.A., J.R. Christensen, E. Barone, C. Suarez, V. Sirotkin and D.R. Kovar. 2014. Homeostatic actin cytoskeleton networks are regulated by assembly factor competition for monomers. Curr Biol. 24:579-585.

Caspari, T., M. Dahlen, G. Kanter-Smoler, H.D. Lindsay, K. Hofmann, K. Papadimitriou, P. Sunnerhagen and A.M. Carr. 2000. Characterization of Schizosaccharomyces pombe Hus1: a PCNA-related protein that associates with Rad1 and Rad9. Mol Cell Biol. 20:1254-1262.

Costello, G., Rodgers, L. and Beach, D. (1986). Fission yeast enters the stationary phase g0 state from either mitotic g1 or g2. Curr. Genet. 11, 119-125.

Coulton, A.T., D.A. East, A. Galinska-Rakoczy, W. Lehman and D.P. Mulvihill. 2010. The recruitment of acetylated and unacetylated tropomyosin to distinct actin polymers permits the discrete regulation of specific myosins in fission yeast. J Cell Sci. 123:3235-3243.

Cox, J., and M. Mann. 2008. MaxQuant enables high peptide identification rates, individualized p.p.b.-range mass accuracies and proteome-wide protein quantification. Nature Biotechnology. 26:1367-1372.

Cox, J., N. Neuhauser, A. Michalski, R.A. Scheltema, J.V. Olsen, and M. Mann. 2011. Andromeda: a peptide search engine integrated into the MaxQuant environment. Journal of proteome research. 10:1794-1805.

Doyle, A, 2009 R., Martín-García, A. T. Coulton, S. Bagley and **D. P. Mulvihill** (2009) “The fission yeast type V myosin Myo51, is a meiotic spindle pole body component, with discrete roles during cell fusion and spore formation” Journal of Cell Science. **122**: 4330-4340

Elias, J.E., and S.P. Gygi. 2007. Target-decoy search strategy for increased confidence in large-scale protein identifications by mass spectrometry. Nat Methods. 4:207-214.

Fantes, P. 1977. Control of cell size and cell cycle time in Schizosaccharomyces pombe. Journal of Cell Science. 24:51-67.

Fennessy, D., A. Grallert, A. Krapp, A. Cokoja, A.J. Bridge, J. Petersen, A. Patel, V.A. Tallada, E. Boke, B. Hodgson, V. Simanis, and I.M. Hagan. 2014. Extending the Schizosaccharomyces pombe Molecular Genetic Toolbox. PLoS One. 9:e97683.

Hartmuth, S., and J. Petersen. 2009. Fission yeast Tor1 functions as part of TORC1 to control mitotic entry through the stress MAPK pathway following nutrient stress. Journal of Cell Science. 122(Pt 11):1737-46.:1737-1746.

Hayashi, T., M. Hatanaka, K. Nagao, Y. Nakaseko, J. Kanoh, A. Kokubu, M. Ebe, and M. Yanagida. 2007. Rapamycin sensitivity of the Schizosaccharomyces pombe tor2 mutant and organization of two highly phosphorylated TOR complexes by specific and common subunits. Genes Cells. 12:1357-1370.

Hsu, P.P., S.A. Kang, J. Rameseder, Y. Zhang, K.A. Ottina, D. Lim, T.R. Peterson, Y. Choi, N.S. Gray, M.B. Yaffe, J.A. Marto, and D.M. Sabatini. 2011. The mTOR-regulated phosphoproteome reveals a mechanism of mTORC1-mediated inhibition of growth factor signaling. Science. 332:1317-1322.

Huang, J., Y. Huang, H. Yu, D. Subramanian, A. Padmanabhan, R. Thadani, Y. Tao, X. Tang, R. Wedlich-Soldner, and M.K. Balasubramanian. 2012. Nonmedially assembled F-actin cables incorporate into the actomyosin ring in fission yeast. The Journal of cell biology. 199:831-847.

Ikai, N., N. Nakazawa, T. Hayashi, and M. Yanagida. 2011. The reverse, but coordinated, roles of Tor2 (TORC1) and Tor1 (TORC2) kinases for growth, cell cycle and separase-mediated mitosis in Schizosaccharomyces pombe. Open Biology. 1.

Jacinto, E., R. Loewith, A. Schmidt, S. Lin, M.A. Ruegg, A. Hall, and M.N. Hall. 2004. Mammalian TOR complex 2 controls the actin cytoskeleton and is rapamycin insensitive. Nat Cell Biol. 6:1122-1128.

Kowalczyk , K.M. and J. Petersen. 2016. Fission yeast SCYL1/2 homologue Ppk32: a novel regulator of TOR signalling that governs survival during Brefeldin A induced stress to protein trafficking. PLOS Genetics 10.1371/journal.pgen.1006041

Kawai, M., A. Nakashima, M. Ueno, T. Ushimaru, K. Aiba, H. Doi, and M. Uritani. 2001. Fission yeast tor1 functions in response to various stresses including nitrogen starvation, high osmolarity, and high temperature. Current genetics. 39:166-174.

Koch, A., K. Krug, S. Pengelley, B. Macek, and S. Hauf. 2011. Mitotic substrates of the kinase aurora with roles in chromatin regulation identified through quantitative phosphoproteomics of fission yeast. Science signaling. 4:rs6.

Kovar, D.R., J.Q. Wu, and T.D. Pollard. 2005. Profilin-mediated competition between capping protein and formin Cdc12p during cytokinesis in fission yeast. Mol Biol Cell. 16:2313-2324.

Lancaster, O.M., and B. Baum. 2014. Shaping up to divide: coordinating actin and microtubule cytoskeletal remodelling during mitosis. Seminars in cell & developmental biology. 34:109-115.

Laplante, M., and D.M. Sabatini. 2012. mTOR signaling in growth control and disease. Cell. 149:274-293.

Lee, S., F.I. Comer, A. Sasaki, I.X. McLeod, Y. Duong, K. Okumura, J.R. Yates, 3rd, C.A. Parent, and R.A. Firtel. 2005. TOR complex 2 integrates cell movement during chemotaxis and signal relay in Dictyostelium. Mol Biol Cell. 16:4572-4583.

Liu, L., Y. Luo, L. Chen, T. Shen, B. Xu, W. Chen, H. Zhou, X. Han, and S. Huang. 2010. Rapamycin inhibits cytoskeleton reorganization and cell motility by suppressing RhoA expression and activity. J Biol Chem. 285:38362-38373.

Liu, L., and C.A. Parent. 2011. Review series: TOR kinase complexes and cell migration. The Journal of cell biology. 194:815-824.

Matsuo, T., Y. Otsubo, J. Urano, F. Tamanoi, and M. Yamamoto. 2007. Loss of the TOR kinase Tor2 Mimics Nitrogen Starvation and Activates the Sexual Development Pathway in Fission Yeast. Mol Cell Biol.

Motegi, F., R. Arai, and I. Mabuchi. 2001. Identification of two type V myosins in fission yeast, one of which functions in polarized cell growth and moves rapidly in the cell. Mol Biol Cell. 12:1367-1380.

Mulvihill, D.P., T.Z. Win, T. Pack, and J. S. Hyams. (2000) “Cytokinesis in Fission Yeast: A Myosin pas de deux.” Microscopy Research and Technique **49**: 152-160.
Mulvihill, D.P., and J.S. Hyams. 2002. Cytokinetic actomyosin ring formation and septation in fission yeast are dependent on the full recruitment of the polo-like kinase Plo1 to the spindle pole body and a functional spindle assembly checkpoint. J Cell Sci. 115:3575-3586.
Mulvihill, D.P., and J. S. Hyams. (2003) “Role of the two type II myosins, Myo2 and Myp2, in cytokinetic actomyosin ring formation and function in fission yeast.” Cell Motility and the Cytoskeleton. 54: 208-216.
Nakano, K., and I. Mabuchi. 2006. Actin-capping protein is involved in controlling organization of actin cytoskeleton together with ADF/cofilin, profilin and F-actin crosslinking proteins in fission yeast. Genes Cells. 11:893-905.
Neumann, F. R., and P. Nurse P. 2006. Nuclear size control in fission yeast. J Cell Biol. 179: 593-600.
Olsen, J.V., L.M. de Godoy, G. Li, B. Macek, P. Mortensen, R. Pesch, A. Makarov, O. Lange, S. Horning, and M. Mann. 2005. Parts per million mass accuracy on an Orbitrap mass spectrometer via lock mass injection into a C-trap. Mol Cell Proteomics. 4:2010-2021.
Pearson, R.B., and B.E. Kemp. 1991. Protein kinase phosphorylation site sequences and consensus specificity motifs: tabulations. Methods Enzymol. 200:62-81.
Petersen, J., and I.M. Hagan. 2005. Polo kinase links the stress pathway to cell cycle control and tip growth in fission yeast. Nature. 435:507-512.
Rappsilber, J., M. Mann, and Y. Ishihama. 2007. Protocol for micro-purification, enrichment, pre-fractionation and storage of peptides for proteomics using StageTips. Nature protocols. 2:1896-1906.
Riedl, J., A.H. Crevenna, K. Kessenbrock, J.H. Yu, D. Neukirchen, M. Bista, F. Bradke, D. Jenne, T.A. Holak, Z. Werb, M. Sixt, and R. Wedlich-Soldner. 2008. Lifeact: a versatile marker to visualize F-actin. Nat Methods. 5:605-607.
Sarbassov, D.D., S.M. Ali, D.H. Kim, D.A. Guertin, R.R. Latek, H. Erdjument-Bromage, P. Tempst, and D.M. Sabatini. 2004. Rictor, a novel binding partner of mTOR, defines a rapamycin-insensitive and raptor-independent pathway that regulates the cytoskeleton. Curr Biol. 14:1296-1302.
Schmidt, A., J. Kunz, and M.N. Hall. 1996. TOR2 is required for organization of the actin cytoskeleton in yeast. Proc Natl Acad Sci U S A. 93:13780-13785.
Schroeder, M.J., J. Shabanowitz, J.C. Schwartz, D.F. Hunt, and J.J. Coon. 2004. A neutral loss activation method for improved phosphopeptide sequence analysis by quadrupole ion trap mass spectrometry. Analytical chemistry. 76:3590-3598.
Skau, C.T., and D.R. Kovar. 2010. Fimbrin and tropomyosin competition regulates endocytosis and cytokinesis kinetics in fission yeast. Curr Biol. 20:1415-1422.
Skoumpla, K., A.T. Coulton, W. Lehman, M.A. Geeves, and D.P. Mulvihill. 2007. Acetylation regulates tropomyosin function in the fission yeast Schizosaccharomyces pombe. J Cell Sci. 120:1635-1645.
Suarez, C., R.T. Carroll, T.A. Burke, J.R. Christensen, A.J. Bestul, J.A. Sees, M.L. James, V. Sirotkin, and D.R. Kovar. 2015. Profilin regulates F-actin network homeostasis by favoring formin over Arp2/3 complex. Developmental cell. 32:43-53.
Tatebe, H., S. Morigasaki, S. Murayama, C.T. Zeng, and K. Shiozaki. 2010. Rab-family GTPase regulates TOR complex 2 signaling in fission yeast. Curr Biol. 20:1975-1982.
Vazquez-Martin, A., C. Oliveras-Ferraros, L. Bernado, E. Lopez-Bonet, and J.A. Menendez. 2009. The serine 2481-autophosphorylated form of mammalian Target Of Rapamycin (mTOR) is localized to midzone and midbody in dividing cancer cells. Biochemical and biophysical research communications. 380:638-643.

Weisman, R., and M. Choder. 2001. The fission yeast TOR homolog, tor1+, is required for the response to starvation and other stresses via a conserved serine. J Biol Chem. 276:7027-7032.

Win, T.Z., Y. Gachet, D.P. Mulvihill, K.M. May, and J.S. Hyams. 2001. Two type V myosins with non-overlapping functions in the fission yeast Schizosaccharomyces pombe: Myo52 is concerned with growth polarity and cytokinesis, Myo51 is a component of the cytokinetic actin ring. J Cell Sci. 114:69-79.

Wu, J.Q., J.R. Kuhn, D.R. Kovar, and T.D. Pollard. 2003. Spatial and temporal pathway for assembly and constriction of the contractile ring in fission yeast cytokinesis. Developmental Cell. 5:723-734.

Wullschleger, S., J. Loewith, and M. Hall. 2006. TOR signalling in Growth and Metabolism. Cell. 124:471-484.

Yamashita, A., K. Maeda, and Y. Maeda. 2003. Crystal structure of CapZ: structural basis for actin filament barbed end capping. EMBO J. 22:1529-1538.